Electronic Supplementary Material (ESI) for Inorganic Chemistry Frontiers.

Supporting Information

Dual-heteroatom-templated lanthanoid-inserted heteropolyoxotungstates simultaneously comprising Dawson and Keggin subunits and their composite film applied for electrochemical immunosensing auximone

Saisai Xie, Dan Wang,* Zixu Wang, Jiancai Liu, Lijuan Chen,* and Junwei Zhao*

Henan Key Laboratory of Polyoxometalate Chemistry, College of Chemistry and Chemical Engineering, Henan University, Kaifeng 475004, China

Fig. S1. IR spectra of **1** (up) and **2** (down).

Fig. S2. (a-b) Comparisons of experimental PXRD and their corresponding simulated XRD patterns of **1** and **2**.

Fig. S3. TG curves of **1** and **2**.

Fig. S4. (a) XPS spectrum of the P^{III} element in **1.** (b) XPS spectrum of the P^{III} element in **2**.

Fig. S5. CV curves of the bare GCE and modified GCEs prepared by Pyrrole, **1**+Pyrrole, $\{SbW_9\}$+Pyrrole in 0.20 M CH_3COOH−CH_3COONa buffer (pH = 4.5).

Fig. S6. (a) SEM of the **1**@PPY film (120 s). (b) Cross-section SEM of the **1**@PPY film (120 s). (c) SEM of the **1**@PPY film (360 s). (d) Cross-section SEM of the **1**@PPY film (360 s).

Fig. S7. (a) XPS survey spectrum of the **1**@PPY film. (b–d) XPS spectra of W4f, C1s, and N1s in the **1**@PPY film on ITO glass (240 s).

Fig. S8. EDS of the **1**@PPY film (240 s) on ITO glass.

Fig. S9. The SEM elemental mapping images of the **1**@PPY film (240 s).

Fig. S10. (a) DPV curves of **1**@PPY/GCE films stored for different times. (b) DPV curves of bare GCE stored for different times. DPV curves were measured in Fe−1 solution.

Fig. S11. IR spectra of **1** (up) and Cs-**1** (down).

Fig. S12. SEM elemental mapping images of the Au/**1**@PPY film (240 s).

Fig. S13. EIS spectra of the modified electrodes by different materials in Fe−2 solution. (A: bare GCE; B: **1**@PPY/GCE; C: Au/**1**@PPY/GCE; D: anti-IAA/Au/**1**@PPY/GCE; E: IAA/anti-IAA/Au/**1**@PPY/GCE.

Fig. S14. (a) DPV curves of the **1** and **2**. DPV were conducted in Fe−1 solution. (b) DPV curves of the IAA/anti-IAA/Au/**1**@PPY/GCE and IAA/anti-IAA/Au/**2**@PPY/GCE. DPV were conducted in Fe−2 solution.

Fig. S15. (a) DPV curves for anti-IAA/Au/**1**@PPY/GCEs with the IAA concentration varying from 0 $pg{\cdot}mL^{-1}$ to $1{\times}10^5$ $pg{\cdot}mL^{-1}$. (b) DPV curves for anti-IAA/Au/**1**@PPY/GCE in the presence of different interferents. (c) DPV curves of **1**@PPY biosensor detecting mixed interferents (a = IAA+ABA, b =IAA+SA, c = IAA+GL, d = IAA+ABA+SA+GL). DPV tests were conducted in Fe−2 solution.

Fig. S16. (a) DPV curves of six IAA/anti-IAA/Au/**1**@PPY/GCEs. (b) The stability of the **1**@PPY/GCEs with varying days. DPV tests were conducted in Fe−2 solution.

Table S1. Summary of synthesis methods about some typical antimonotungstates.

Table S2. Crystallographic data and structure refinements for **1** and **2**.

Table S3. Comparison of the sensitivity of different sensors for monitoring IAA.

Materials and physical measurements

The $Na_9[B\text{-}\alpha\text{-}SbW_9O_{33}]\cdot 19.5H_2O$ precursor was synthesized according to the previous reference.[1] IAA, abscisic acid (ABA), salicylic acid (SA), potassium ferricyanide ($K_3[Fe(CN)_6]$), chloroauric acid ($HAuCl_4$) were purchased from Aladdin (Shanghai, China). Phosphate buffer solutions (PBS) were prepared by mixing the stock solution of 0.1 M NaH_2PO_4 and 0.1 M Na_2HPO_4, and the pH was adjusted by using NaOH or HCl. C, H and N elemental contents were performed on a Perkin–Elmer 240C element analyzer. Inductively coupled plasma mass spectrometry was conducted on a Perkin–Elmer NexION 2000 ICP mass spectrometer. IR spectra were recorded on a Bruker VERTEX 70 IR spectrometer using KBr pellets in the range of 400–4000 cm^{-1}. PXRD patterns were collected on a Bruker D8 ADVANCE apparatus using Cu Kα radiation (λ = 1.54056 Å) with a scan range (2θ) of 3.5 – 50° at 293 K. TG analyses were conducted under N_2 atmosphere on a Mettler–Toledo TGA/SDTA 851^e thermal analyzer (temperature range: 25–1000 °C; heating rate: 10 °C·min^{-1}). SEM images and EDS patterns were obtained by FESEM, Zeiss Gemini 500. All the samples for SEM and EDS characterization were prepared on the indium tin oxide conductive glass (1 × 5 × 20 mm^3). Atomic force microscopy images were collected on a scanning probe microscope SPM-9700HT (Shimadzu). Raman spectroscopy was performed on Edinburgh RM5.

X-ray crystallography

Diffraction intensity data of **1** and **2** were collected on a Bruker D8 Venture Photon II diffractometer using monochromated Mo Kα radiation (λ = 0.71073 Å) at 296 K. Routine Lorentz and polarization corrections were applied and a multi-scan absorption correction was utilized with the SADABS program. Direct methods were used to solve the structures, refined on F^2 by full-matrix least-squares method, using the SHELXTL–97 program.[2,3] All H atoms connected to N and C atoms were generated geometrically and refined isotropically as a riding model using the default SHELXTL parameters. No hydrogen atoms associated with water molecules are located from the difference Fourier map. All non-hydrogen atoms are refined anisotropically except for some oxygen atoms and water molecules. However, there are still solvent accessible voids accessible solvent voids in the check cif reports of crystal structures, suggesting that some lattice water molecules and counter cations should exist in the structures, which can't be found from the weak residual electron peaks. On the basis of elemental analysis and TG analysis, 4 $[H_2(CH_3)_2]^+$ cations, 9 protons and 16 lattice water molecules were directly added to the molecular formula of **1** and **2**. The crystallographic data and structure refinements for **1** and **2** are demonstrated in Table S2. Crystallographic data for **1** and **2** reported in this paper have been deposited in the Cambridge Crystallographic Data Centre with CCDC 2106805 for **1** and 2106806 for **2**.

Synthesis of 1

$Na_2WO_4\cdot 2H_2O$ (5.000 g, 15.159 mmol), $Na_9[B\text{-}\alpha\text{-}SbW_9O_{33}]\cdot 19.5H_2O$ (1.000g, 0.350mmol), DL-malic acid (0.400g, 2.983 mmol), H_3PO_3 (0.040g, 0.488 mmol), and dimethylamine hydrochloride (1.750 g, 21.472 mmol) were dissolved in 25.00 ml of distilled water upon stirring, and the pH value of the clear solution was adjusted to 3.00 by 6.00 M HCl. After the solution was stirred for 20 min, $Nd(CH_3COO)_3$ (0.350g, 1.104mmol) was added. The resulting solution was stirred for around 20 min. The final pH value of the solution was kept at 3.00 by addition of 6.00 M HCl. After constant stirring for another 30 min. Eventually, the solution was placed in a 90 °C water bath for 2 h. Slow evaporation of the solution resulted in light purple rectangular crystals after about one week. Elemental analysis (%): C, 2.84 (cald. 2.64); H, 1.51

(cald. 1.39); N, 0.96 (cald. 0.86); P, 0.47 (cald. 0.38); Sb, 3.11 (cald. 2.98), Na, 0.21 (cald. 0.14); W, 61.72 (cald. 61.91); Nd, 3.63 (cald. 3.53).

Synthesis of 2

The synthetic procedure of **2** is similar to that of **1** except that $Nd(CH_3COO)_3$ (0.310 g, 1.104 mmol) was replaced by $Pr(CH_3COO)_3$ (0.310 g, 1.104 mmol). Light green rectangular crystals of **2** were obtained. Elemental analysis (%): C, 2.86 (cald. 2.65); H, 1.61 (cald. 1.39); N, 0.92 (cald. 0.86); P, 0.42 (cald. 0.38); Sb, 3.09 (cald. 2.99); Na, 0.20 (cald. 0.14); W, 61.83 (cald. 61.96); Pr, 3.54 (cald. 3.45).

Preparation and characterization of 1@PPY film

The polymerization process for preparing the **1**@PPY film was conducted by the chronoamperometric technique in a solution containing 5.0 mM **1** and 7.0mM PY under a 0.65 V applied potential (vs Ag/AgCl) for a certain time (0 / 40 / 80 /120 /180 / 240/ 300 /360 s). AFM, SEM and XPS tests were carried out with ITO as the substrate for the **1**@PPY film. The cyclic voltammetry (CV) test (scan rate: 0.1 V/s) of bare GCE and GCE modified by different materials were carried out in CH_3COOH–CH_3COONa buffer (pH = 4.5). The differential pulse voltammetry (DPV) measurement (amplitude: 0.05 V) of **1**@PPY/GCE was performed in Fe−1 solution (0.10 M PBS, pH = 7.4, 0.01 M $K_3[Fe(CN)_6]/K_4[Fe(CN)_6]$ ($n(Fe^{2+}):n(Fe^{3+})$ = 1:1), 1.00 M KCl) at room temperature. The electrochemical studies were all carried out on a CHI66D electrochemical workstation. A conventional three-electrode system consisting of a glassy carbon electrode (GCE) with a diameter of 3 mm or indium tin oxide (ITO) glass as the working electrode, Ag/AgCl as the reference electrode and a platinum electrode as the counter electrode. All potentials in this work are referenced to the Ag/AgCl electrode.

Preparation of 1@PPY/GCE

Electrochemical polymerization of the **1**@PPY film on GCE was achieved by the chronoamperometric technique in a solution containing 5.0 mM **1** and 7.0 mM pyrrole for 0/40/80/120/180/240/ 300/360 s respectively in Fe−1 solution and the final selected time is 240 s.

Preparation of the Au/1@PPY/GCE

NGPs were site-specifically deposited onto the **1**@PPY electrode in $AuCl_4^-$ solution at −0.2 V (*vs* Ag/AgCl) for 20/40/60/80/100/120 s, obtaining the Au-modified **1**@PPY electrodes (Au/**1**@PPY/GCEs), which provided a necessary condition for further combining the anti-IAA through Au–S bond interaction. $AuCl_4^-$ solution: 1 mL 10.00 $g{\cdot}L^{-1}$ $HAuCl_4$ solution and 1.01 g KNO_3 were used to prepare 100.00 ml $AuCl_4^-$ solution with high purity water.

Preparation of the anti-IAA/Au/1@PPY/GCE

10.00 μL anti-IAA (0.01 mg/ml) was dropped on the Au/**1**@PPY/GCE surface and were maintained for 0/1/2/3/4/5 h at room temperature under humid conditions. After the anti-IAA/Au/**1**@PPY/GCE was washed with ultrapure water, the modified electrode was then immersed in 16 μL of 0.01 mg mL^{-1} BSA for 30 min to eliminate the nonspecific binding anti-IAA.

Electrochemical detection of IAA by anti-IAA/Au/1@PPY/GCE

For IAA detection, 10 μL of IAA standard solution with different concentrations (0 / 1×10^2 / 1×10^3 / 5×10^3 / 1×10^4 / 5×10^4 / 1×10^5 pg·mL^{-1}) were dropped onto the surface of the modified electrodes and incubated for 1 h under humid conditions.

Optimization of experimental conditions

(1) The NGP electrodeposition time. DPV measurements of Au/**1**@PPY electrodes with different electrodeposition times of NGPs in the range of 20 – 120 s have been performed in Fe−2 solution. (2) The incubation time of anti-IAA. The anti-IAA/Au/**1**@PPY/GCE electrodes incubated by different times of anti-IAA were prepared and studied by making use of DPV measurements in Fe−2 solution. The optimal choices were acquired as follows: (1) The NGP electrodeposition time was determined as 80 s; (2) The incubation time of anti-IAA was selected as 3 h.

Electrochemical measurements in immunosensor construction

All electrochemical experiments were conducted on a CHI66D electrochemical workstation. A conventional three-electrode system consisted of a glassy carbon electrode (GCE) with a diameter of 3 mm as the working electrode, Ag/AgCl as the reference electrode and a platinum electrode as the counter electrode. DPV (amplitude: 0.05 V) and electrochemical impedance spectroscopy (EIS; amplitude: 5 mV) data were collected in Fe−2 solution (0.10 M PBS, pH 7.4, 5.00 mM $K_3[Fe(CN)_6]$) at room temperature. The reduced peak current of $[Fe(CN)_6]^{3-}$ obtained by DPV was used to evaluate the immunosensor performance and construct a calibration curve.

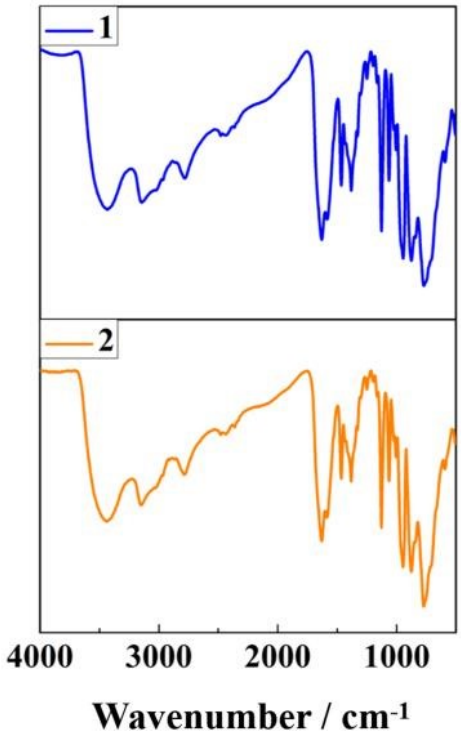

Fig. S1. IR spectra of **1** (up) and **2** (down).

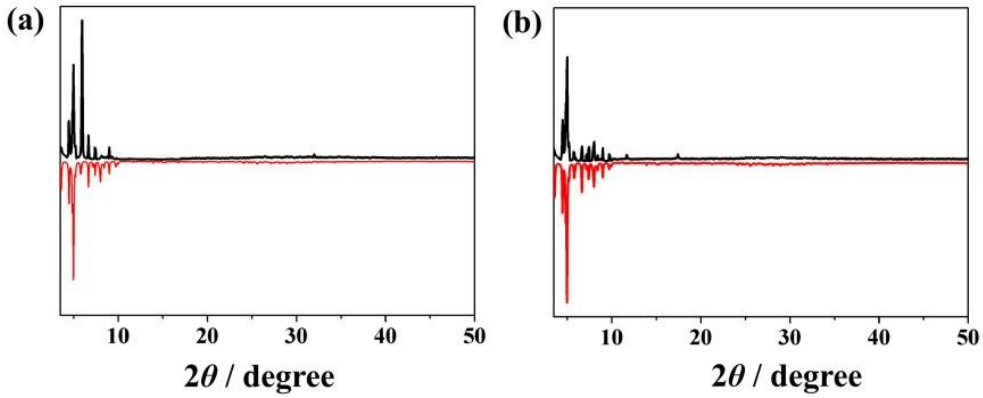

Fig. S2. (a-b) Comparisons of experimental PXRD and their corresponding simulated XRD patterns of **1** and **2**.

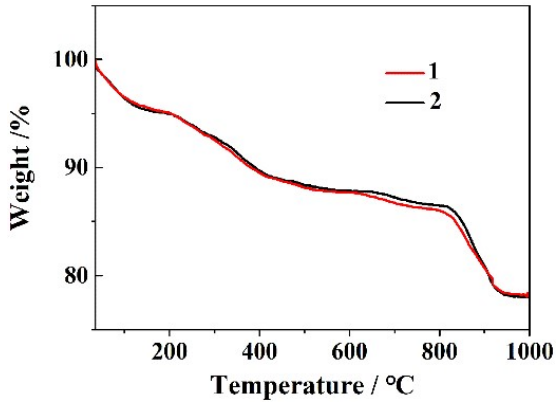

Fig. S3. TG curves of **1** and **2**.

TG analyses of **1**–**2** have been conducted. It can be seen from the TG curves that the weight loss procedure of **1** and **2** can be divided into two steps: The first weight loss (4.91 % for **1**, 4.91% for **2**) happens when the temperature reaches 200 °C, resulting from the release of forty-four lattice water molecules (calcd. 4.93 % (**1**), 4.93 % (**2**),). With temperature increasing, the removal of ten dimethylamine groups, four H_2MA^- ligands, fourteen coordinated water molecules and the dehydration of nine protons during the temperature range of 200–800 °C, leading to the second weight loss of 9.05% for **1**, 8.62% for **2**, (calcd. 8.41% for **1**, 8.42% for **2**). Subsequently, the skeletons of **1**–**2** begin to collapse as the temperature further increases and the WO_3 is sublimated.[4]

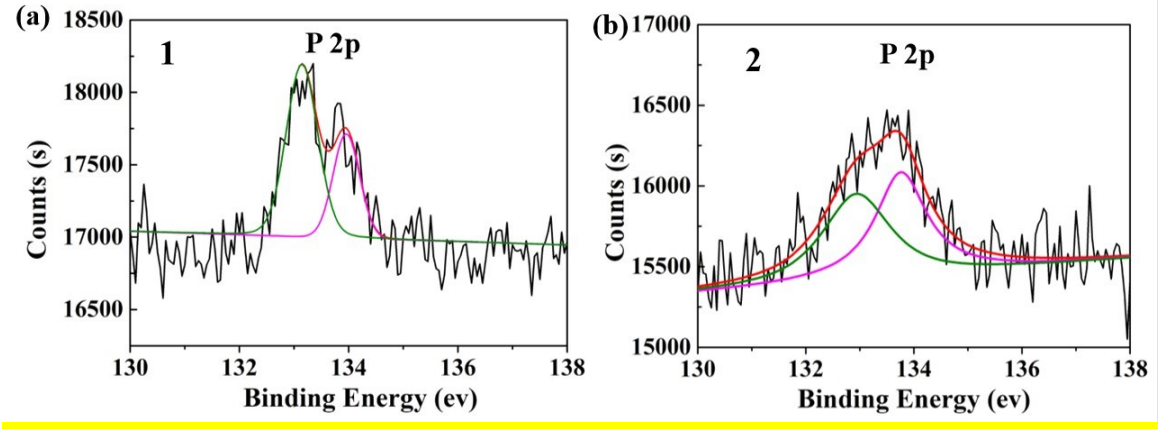

Fig. S4. (a) XPS spectrum of the P^{III} element in **1.** (b) XPS spectrum of the P^{III} element in **2**.

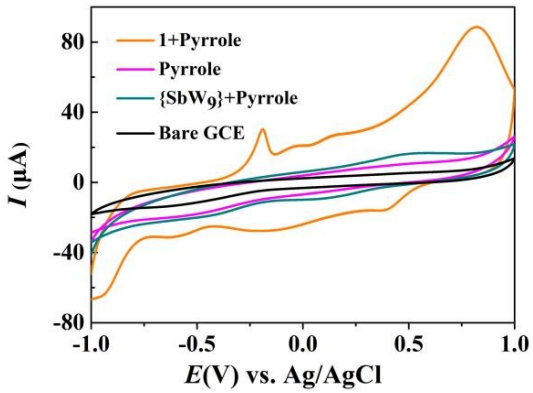

Fig. S5. CV curves of the bare GCE and modified GCEs prepared by Pyrrole, **1**+Pyrrole, $\{SbW_9\}$+Pyrrole in 0.20 M CH_3COOH–CH_3COONa buffer (pH = 4.5).

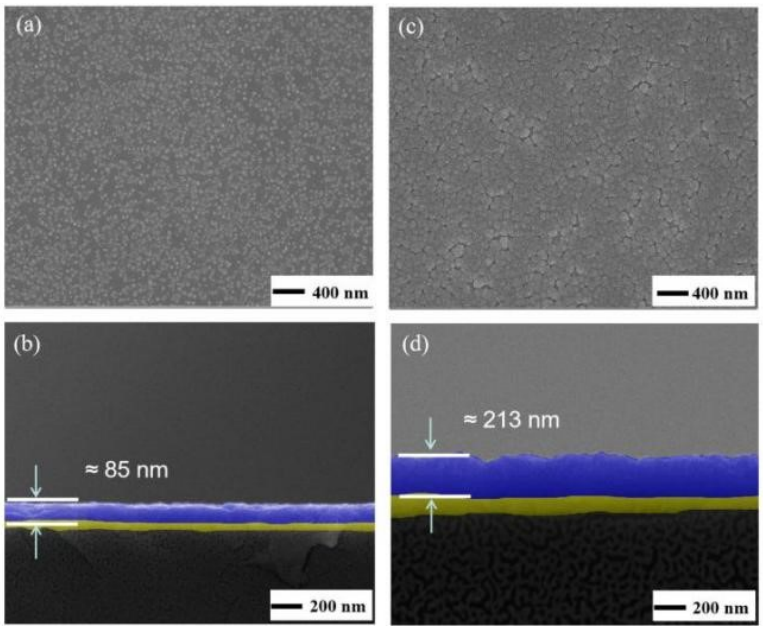

Fig. S6. (a) SEM of the **1**@PPY film (120 s). (b) Cross-section SEM of the **1**@PPY film (120 s). (c) SEM of the **1**@PPY film (360 s). (d) Cross-section SEM of the **1**@PPY film (360 s).

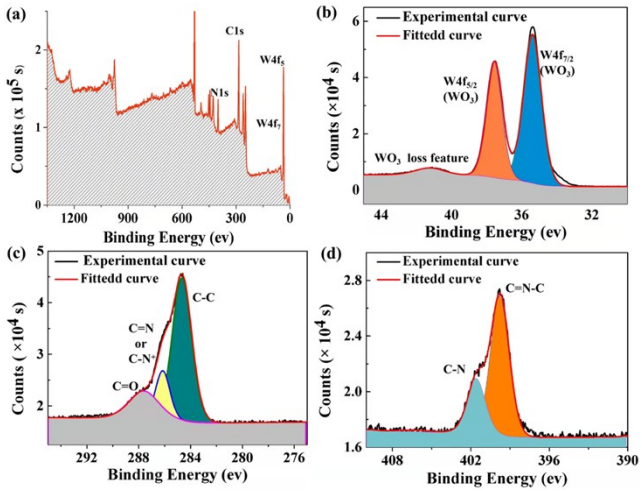

Fig. S7. (a) XPS survey spectrum of the **1**@PPY film. (b–d) XPS spectra of W4f, C1s, and N1s in the **1**@PPY film on ITO glass (240 s).

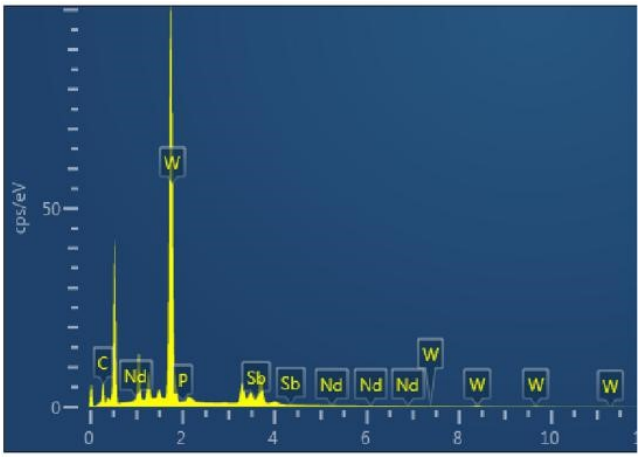

Fig. S8. EDS of the **1**@PPY film (240 s) on ITO glass.

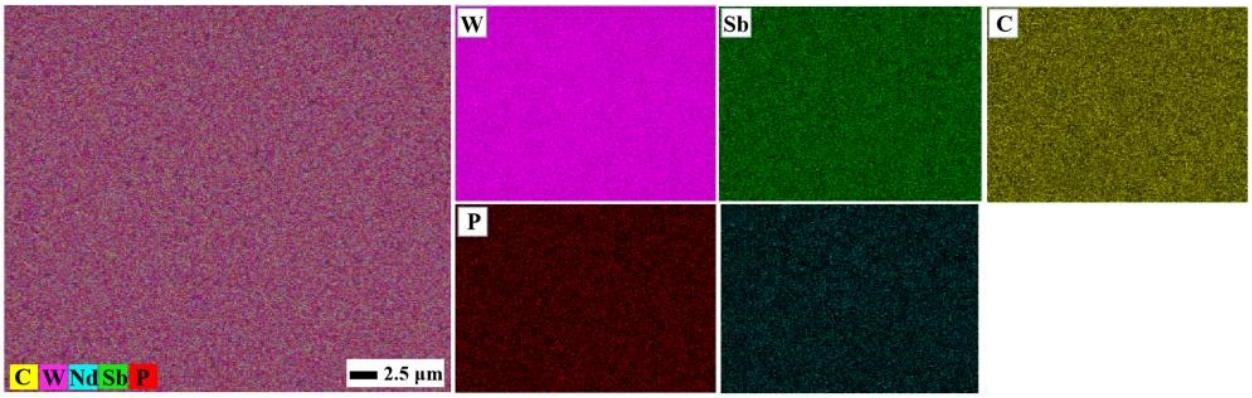

Fig. S9. The SEM elemental mapping images of the **1**@PPY film (240 s).

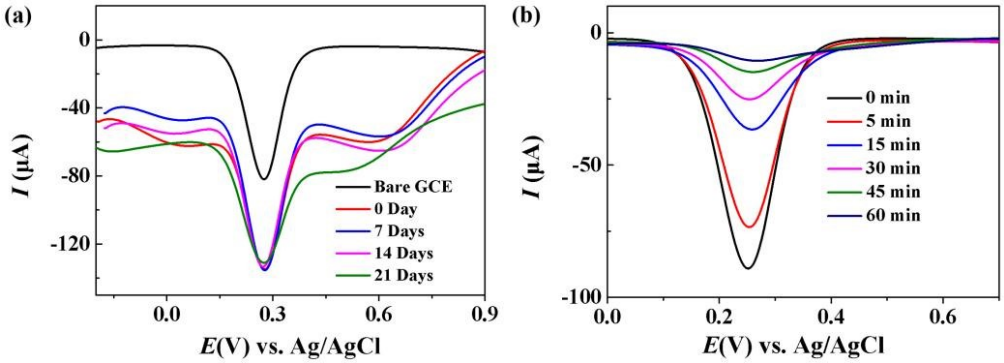

Fig. S10. (a) DPV curves of **1**@PPY/GCE films stored for different times. (b) DPV curves of bare GCE stored for different times. DPV curves were measured in Fe−1 solution.

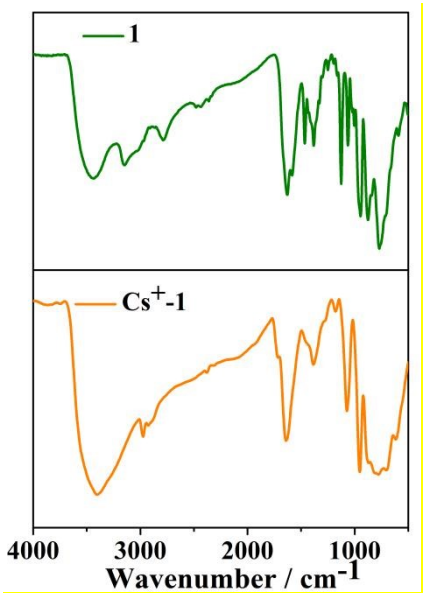

Fig. S11. IR spectra of **1** (up) and Cs-**1** (down).

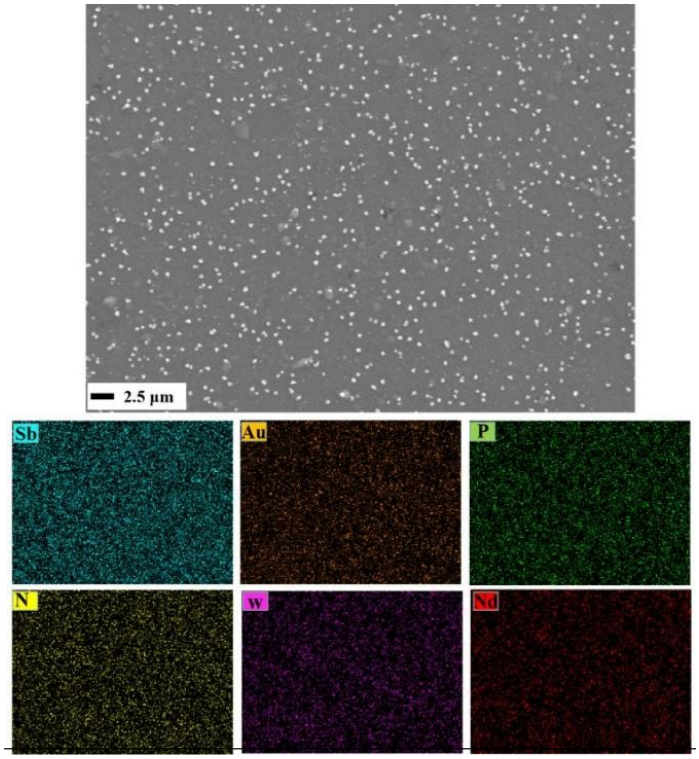

Fig. S12. SEM elemental mapping images of the Au/**1**@PPY film (240 s).

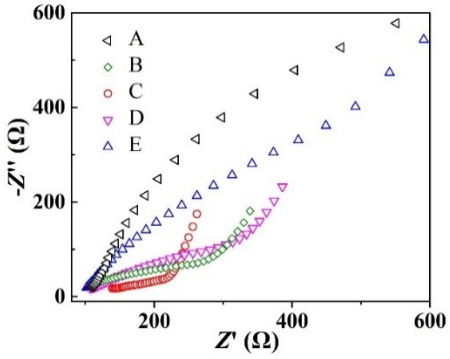

Fig. S13. EIS spectra of the modified electrodes by different materials in Fe−2 solution. (A: bare GCE; B: **1**@PPY/GCE; C: Au/**1**@PPY/GCE; D: anti-IAA/Au/**1**@PPY/GCE; E: IAA/anti-IAA/Au/**1**@PPY/GCE.

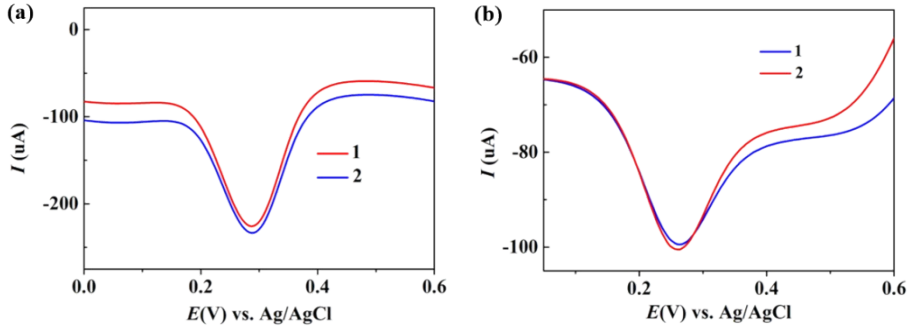

Fig. S14. (a) DPV curves of the **1** and **2**. DPV were conducted in Fe−1 solution. (b) DPV curves of the IAA/anti-IAA/Au/**1**@PPY/GCE and IAA/anti-IAA/Au/**2**@PPY/GCE. DPV were conducted in Fe−2 solution.

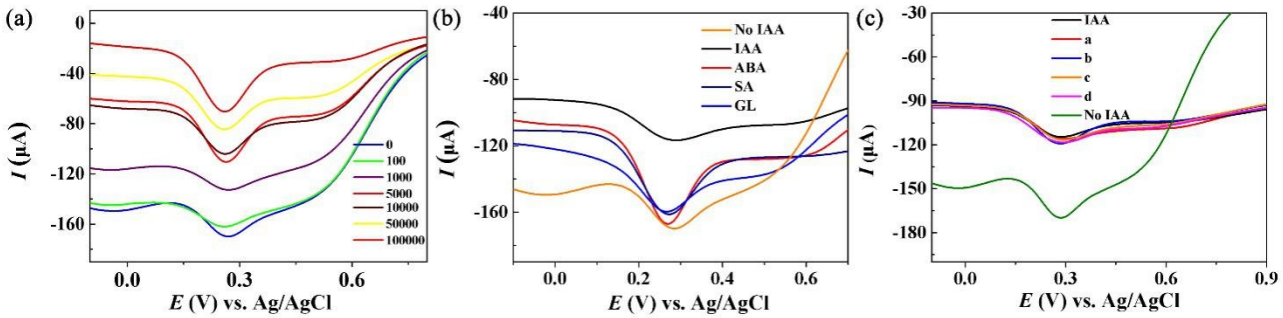

Fig. S15. (a) DPV curves for anti-IAA/Au/**1**@PPY/GCEs with the IAA concentration varying from 0 pg·mL^{-1} to 1×10^{5} pg·mL^{-1}. (b) DPV curves for anti-IAA/Au/**1**@PPY/GCE in the presence of different interferents. (c) DPV curves of **1**@PPY biosensor detecting mixed interferents (a = IAA+ABA, b = IAA+SA, c = IAA+GL, d = IAA+ABA+SA+GL). DPV tests were conducted in Fe−2 solution.

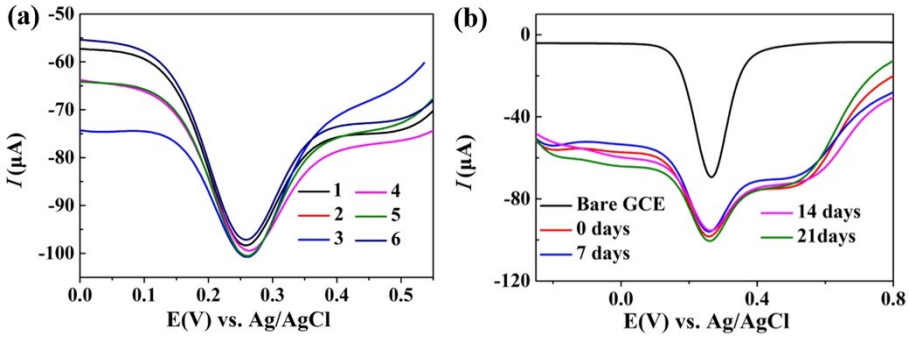

Fig. S16. (a) DPV curves of six IAA/anti-IAA/Au/**1**@PPY/GCEs. (b) The stability of the **1**@PPY/GCEs with varying days. DPV tests were conducted in Fe−2 solution.

Table S1. Summary of synthesis methods about some typical antimonotungstates.

	Molecular Formula	Raw material	Molar ratio	pH	Temperature (°C)	Ref.
Organic-inorganic hybrid antimonotungstates	$[\{Y(\alpha\text{-}SbW_9O_{31}(OH)_2)(CH_3COO)(H_2O)\}_3(WO_4)]^{17-}$	$Na_2WO_4.2H_2O$, $Na_9SbW_9O_{33}\cdot19.5H_2O$, YCl_3, 1 M LiOAc/AcOH	{SbW_9}:W:LN:OL* = 3:1:3:80	5.3	80	5
	$[Ln_2(H_2O)_4\{WO_2(pic)\}_2(SbW_8O_{30})_2]^{10-}$ (LN = La^{3+}, Pr^{3+})	$Ln(NO_3)_3.6H_2O$, 2-Picolinic acid, $Na_9SbW_9O_{33}\cdot19.5H_2O$	{SbW_9}:Ln:OL = 1:1:2	5.0	90	6
	$[\{Ln(H_2O)\}\{Ln(pic)\}(Sb_3O_4)(SbW_8O_{31})(SbW_{10}O_{35})]_2^{24-}$ (Ln=Tb^{3+}, Dy^{3+},Ho^{3+} , Hpic = 2-picolinic acid)					
	$[Eu_3(CH_3COO)_3(HPO_3)(WO_4)][B\text{-}\alpha\text{-}SbW_9O_{33}]_3^{25-}$	$Na_9SbW_9O_{33}\cdot19.5H_2O$, $Na_2WO_4\cdot2H_2O$, H_3PO_3, $Eu(NO_3)_3\cdot6H_2O$	{SbW_9}:W:Ln:OL = 2.013:1:1.455:49.423	5.5	90	7
DHA-POMs	$[Ln_3Ni_9(\mu_3\text{-}OH)_9(SbW_9O_{33})_2(P^VW_9O_{34})_3(CH_3COO)_3]^{30-}$	$Na_9SbW_9O_{33}\cdot19.5H_2O$, $NiCl_2\cdot6H_2O$, $Dy(NO_3)_3\cdot5H_2O$, KH_2PO_4	P:{SbW_9}:Ln = 4.536:1.0595:1		80	8
	$[Ln_2(H_2O)_7(W_4O_9)(HPSeW_{15}O_{54})(SeW_9O_{33})_2]^{14-}$ (Ln = Ce^{3+}, Pr^{3+}, Nd^{3+}, Sm^{3+}, Gd^{3+}, Tb^{3+}, Ho^{3+}, Er^{3+})	$Na_2WO_4\cdot2H_2O$, DMA·HCl, Na_2SeO_3 H_3PO_3, $Ce(NO_3)_3\cdot6H_2O$	P:Se:Ln:W = 2.902:1:1.402:10.449	3.2	90	9
Organic-inorganic hybrid-DHA-POMs	$[Ln_4(HP^{III})W_8(H_2O)_{12}(H_2ptca)_2O_{28}][Sb^{III}W_9O_{33}]_2^{12-}$ (Ln = Ce^{3+}, La^{3+}, Pr^{3+}, H_2ptca= 1,2,3-propanetricarboxylic acid)	$Na_9SbW_9O_{33}\cdot19.5H_2O$, H_3PO_3, 1,2,3-propanetricarboxylic acid DMA·HCl	P:{SbW9}:Ln:OL = 2.566:1.798:1:3.226	4.0	90	10
	$[Ln_4(H_2O)_{14}W_7O_{15}(H_2MA)_4][Sb^{III}W_9O_{33}]_2[HP^{III}Sb^{III}W_{15}O_{54}]_2^{20-}$ (Ln = Nd^{3+}, Pr^{3+}, H_3MA=DL-Malic Acid)	$Na_2WO_4\cdot2H_2O$, $Na_9SbW_9O_{33}\cdot19.5H_2O$, H_3PO_3, DMA·HCl, DL-Malic Acid	P:{SbW_9}:W:Ln:OL=35.68:1:43.31 1:3.154:8.523	3.0	90	Our work

* OL=Organic Ligand

Table S2. Crystallographic data and structure refinements for **1** and **2.**

	1	**2**
Empirical formula	$C_{36}H_{227}N_{10}Nd_4NaO_{267}P_2Sb_4W_{55}$	$C_{36}H_{227}N_{10}Pr_4NaO_{267}P_2Sb_4W_{55}$
Fw	16333.92	16320.60
T (K)	150(2)	150(2)
Crystal system	Monoclinic	Monoclinic
Space group	*P*2/*n*	*P*2/*n*
a (Å)	30.1465(8)	30.1932(9)
b (Å)	35.4265(12)	35.4800(12)
c (Å)	34.1200(9)	34.1217(8)
β (deg)	96.4110(10)	106.7680(10)
V (Å3)	36211.8	36323.7
Z	4	4
D_c (g·cm^{-3})	2.910	3.407
μ (mm^{-1})	18.336	18.244
Limiting indices	$-35 \le h \le 35$	$-35 \le h \le 35$
	$-36 \le k \le 42$	$-42 \le k \le 36$
	$-39 \le l \le 40$	$-39 \le l \le 40$
GOF on F^2	1.084	1.058
R_1, wR_2 [I > 2σ(I)]	R_1 = 0.0641, wR_2 = 0.1802	R_1 = 0.0605, wR_2 = 0.1653
R_1, wR_2 [all data]	R_1 = 0.1159, wR_2 = 0.2016	R_1 = 0.1081, wR_2 = 0.1859

Table S3. Comparison of the sensitivity of different sensors for monitoring IAA.

Electrochemical method	LOD	Linear range	Ref.
DPV	0.050 μM	0.1–7.0 μM	11
DPV	0.018 ng·mL^{-1}	0.02–500.00 ng·mL^{-1}	12
Amperometric	0.020 μM	0.10–50.00 μM	13
DPV	87.41 pg·mL^{-1}	100.00-500000.00 pg·mL^{-1}	Our Work

References

1 M. Bösing, I. Loose, H. Pohlmann and B. Krebs, New strategies for the generation of large heteropolymetalate clusters: the β-B-SbW_9 fragment as a multifunctional unit, *Chem. Eur. J.,* 1997, **3**, 1232−1237.

2 G. M. Sheldrick, SHELXL-97, Program for Crystal Structure Refinement, University of Göttingen: Göttingen, Germany, 1997.

3 G. M. Sheldrick, SHELXS-97, Program for Crystal Structure Solution, University of Göttingen: Göttingen, Germany, 1997.

4 J. Wendel. Master Thesis, Lund University, Lund, Sweden, 2014.

5 M. Ibrahim, S. S. Mal, B. S. Bassil, A. Banerjee and U, Kortz, Yttrium(III)-containing tungstoantimonate(III) stabilized by tetrahedral WO_4^{2-} capping unit, $[\{Y(\alpha\text{-}SbW_9O_{31}(OH)_2)(CH_3COO)(H_2O)\}_3(WO_4)]^{17-}$, *Inorg. Chem*., 2011, ***50***, 956−960.

6 L. L. Li, H. Y. Han, Y. H. Wang, H. Q. Tan, H. Y. Zang and Y. G. Li, Construction of polyoxometalates from dynamic lacunary polyoxotungstate building blocks and lanthanide linkers, *Dalton Trans*., 2015, ***44***, 11429−11436.

7 X. Xu, C. T. Lu, S. S. Xie, L. J. Chen and J. W. Zhao, A trimeric tri-Tb 3+ including antimonotungstate and its Eu^{3+}/Tb^{3+}/Dy^{3+}/Gd^{3+}-codoped species with luminescence properties, *Dalton Trans*., 2020, ***49***, 12401−12410.

8 J. Cai, X. Y. Zheng, J. Xie, Z. H. Yan, X. J. Kong, Y. P. Ren, L. S. Long and L. S. Zheng, Anion-dependent assembly of heterometallic 3d–4f clusters based on a lacunary polyoxometalate, *Inorg. Chem*., 2017, **56**, 8439−8445.

9 L. L. Liu, J. Jiang, X. Y. Liu, G. P. Liu, D. Wang, L. J. Chen and J. W. Zhao, First series of mixed (P^{III}, Se^{IV})-heteroatoms oriented rare-earth embedded polyoxotungstates containing distinct building blocks, *Inorg. Chem. Front*., 2020, **46**, 404−651.

10 S. S. Xie, J. Jiang, D. Wang, Z. G. Tang, R. F. Mi, L. J. Chen and J. W. Zhao, Tricarboxylic-ligand-decorated lanthanoid-inserted hetero-polyoxometalates built by mixed-heteroatom-directing polyoxotungstate units: syntheses, structures, and electrochemical sensing for 17β-estradiol, *Inorg. Chem*., 2021, ***60***, 7536−7544.

11 T. Gan, C. G. Hu, Z. L. Chen and S. S. Hu, A disposable electrochemical sensor for the determination of indole-3-acetic acid based on poly (safranine T)-reduced graphene oxide nanocomposite, *Talanta,* 2011, ***85***, 310−316.

12 H. S. Yin, Z. N. Xu, Y. L. Zhou, M. Wang and S. Y. Ai, An ultrasensitive electrochemical immunosensor platform with double signal amplification for indole-3-acetic acid determinations in plant seeds, *Analyst*, 2013, ***138***, 1851−1857.

13 K. B. Wu, Y. Y. Sun and S. S. Hu, Development of an amperometric indole-3-acetic acid sensor based on carbon nanotubes film coated glassy carbon electrode, *Sensor. Actuat. B*. 2003, ***96***, 658−662.